Bulgarian Chemical Communications, Volume 58, Issue 1 (pp. 85-92) 2026 *DOI: 10.34049/bcc.58.1.5699*

Stefan blowing and chemical reaction influences on non-Darcian flow of Casson nanofluid over a stretched surface

M. Gnaneswara Reddy [1], S. Kiranmaiye [1], M. Eswara Rao [2]*

[1] *Department of Mathematics, Narayana Engineering College (Autonomous), Gudur, Tirupati-524 101, Andhra Pradesh, India*

[2] *Department of Mathematics, Saveetha School of Engineering, SIMATS, Chennai, Tamil Nadu, India*

Received: May 05 2025; Revised: November 20, 2025

Studying the magnetohydrodynamic flow, heat and mass transfer properties of a Casson nanofluid flow over an unstable stretched sheet with varying heat and mass fluxes while taking Stefan blowing parameter and non-Darcian porous medium into account is the goal of this paper. The motivation stanches from the prerequisite to comprehend progressive heat and mass transfer characteristics and their insinuations for science, engineering and industrial system. New aspects related to Brownian motion and thermophoresis with heat transfer are examined. The effects of chemical reaction, Eckert number, and thermal radiation are examined in this work. The critical partial differential equations that govern momentum, boundary conditions, concentration, and temperature transform a non-linear ordinary differential equations system by applying suitable similarity transformations. The outcomes of critical physical parameters are acquired by engaging the built-in bvp4c solver in the MATLAB computational software. Comparison shows that the present results are in excellent agreement with previous existing results. The profiles of temperature, velocity, and concentration as well as the related physiological traits used in the study are identified. When the chemical reaction rate manifests, the nanoparticle concentration profile decreases, but the Stefan blowing parameter exhibits the opposite behavior. The intricate relationship between the skin friction coefficient, Sherwood number, and Nusselt number, and their impact on mass and heat transfer characteristics, was a subject of extensive research in various fields, including fluid dynamics, heat transfer, and chemical engineering.

Keywords: Chemical reaction, Stefan blowing, Casson nanofluid, MHD, Thermal radiation.

INTRODUCTION

The Casson fluid model, first introduced by Casson in 1959, has become a popular choice for analyzing the rheological behavior of various non-Newtonian fluids. This model is particularly suitable for describing the flow characteristics of fluids that exhibit yield stress, such as food processing, pharmaceuticals, cosmetics, and materials science. Its particular strength lies in its capacity to clarify the flow properties of materials that undergo a noticeable transition from a solid-like to a fluid-like state when exposed to applied stress [1-6]. The MHD flow of Casson fluid across an inclined permeable stretched surface was examined by Kumar and Srinivas [7] in relation to the combined effects of thermal radiation and Joule heating. Raja *et al*. [8] employed intelligent computing techniques to explore the magnetohydrodynamic (MHD) radiative drift of a Von Kármán Casson nanofluid through a Darcy-Forchheimer medium, incorporating activation energy considerations. In the presence of Stefan blowing or suction, Konai *et al*. [9] embarked the Casson nanofluid flow past a stretched surface. The analysis conducted by Sankari *et al.* [10] on the double stratification of Casson nanofluid over an exponential extending sheet demonstrates a comprehensive exploration, specifically delving into the characteristics of non-Newtonian fluids and the behavior of nanofluids. Elgendi *et al*. [11] explored the properties of a steady flow of an incompressible Casson fluid through a permeable stretched surface. In the presence of anisotropy thermal conductivity, Kumar *et al.* [12] embarked the Casson fluid flow in a permeable channel. Researchers have focused a lot of emphasis on studying MHD flows of non-Newtonian fluids in porous media because of its many potential uses. These include processing of petroleum, and textile, biological systems, heat-storage beds, irrigation problems, and polymer composite industries. Many researchers have investigated various aspects of magnetohydrodynamic flows of non-Newtonian fluids passing through a porous medium, providing valuable insights into the field [13-16]. A numerical study of magnetohydrodynamic boundary layer flow through a stretching surface was conducted by Pantokratoras [17]. The MHD dissipative flow

* To whom all correspondence should be sent:
E-mail: *mannerieswar99@gmail.com*

across a shrinking/ stretching surface was examined by Mishra *et al*. [18] in relation to the combined effects of Joule heating and heat absorption. Haider *et al.* [19] examined the unsteady MHD nanofluid flow past a stretched surface when Stefan blowing or suction was present. Using heat absorption and thermal radiation considerations, Alqahtani *et al.* [20] investigated the magnetohydrodynamic flow of a Casson hybrid nanofluid through a Darcy-Forchheimer medium using intelligent computing approaches. Thenmozhi and Rao [21] investigated the magnetohydrodynamic micropolar fluid through a Darcy-Forchheimer medium using the predictor-corrector FDM technique. In the presence of velocity slip, Ouyang *et al.* [22] embarked the magnetohydrodynamics ternary nanofluid flow over a stretching or shrinking surface. The effects of viscous dissipation and Joule heating on magnetohydrodynamics-hybrid nanofluid flow across non-isothermal stretching or shrinking surfaces were investigated by Idris *et al.* [23].

In many industrial and technical processes, the understanding of mass and heat transfer in chemical reactions is crucial. These processes are widely used in many industrial applications, including food processing, ceramic or glassware manufacturing, and polymer production [24-29]. The squeezing flow of Casson nanofluid across a stretched surface was examined by Noor *et al.* [30] in relation to the combined effects of chemical reaction and Joule heating. Manjunatha *et al.* [31] discussed the importance of convective heat transfer and Stefan blowing in nanofluid flow across a curved stretched sheet with chemical reaction. Abbasi *et al*. [32] engaged in a comprehensive discussion regarding the potential applications of Casson nanomaterials in a radiative binary reactive flow near an oblique stagnation point. This exploration involved considering how these unique materials could be utilized in scenarios where radiative heat transference and chemical reactions play significant parts, particularly regarding activation energy applications. Using nonlinear chemical reaction and Joule heating considerations, Khan *et al*. [33] investigated the magnetohydrodynamic flow of a Casson fluid *via* a permeable moving wedge using clever computing techniques. The MHD flow of a Casson nanofluid across an inclined permeable stretched surface was examined by Srinivas *et al.* [34] in relation to the combined effects of chemical reaction and Joule heating. Saleem *et al.* [35] investigation focused on numerical simulations, bolstered by an advanced computing framework, to analyze the intricate chemical reactions occurring within Casson nanofluids. These fluids are recognized for their non-Newtonian behavior and incorporation of suspended nanoparticles. The impact of ultrasonic waves on a turbulent flow with chemical reactions was numerically investigated by Shateri *et al.* [36]. The study by Razzaq *et al*. [37] emphasized the crucial role of Ohmic dissipation and chemical reactions in the Casson nano liquid flow across a extending surface. A complex and multifaceted area of research with significant implications for various engineering and industrial applications is presented by Hasan *et al*. [38] investigation on the numerical study of MHD nanofluid flow and heat transfer, especially when taking exothermic chemical reactions and radiative heat flux into account. Using chemical reaction and thermo–solutal Marangoni convection, Challa *et al*. [39] investigated the effects of gyrotactic microorganisms on Powell–Eyring nanofluid over an inclined stretched surface.

The use of chemical reactions in the magnetized flow of Casson nanofluid through an overextended sheet has not received much attention. Studying flow, heat, and mass transfer in a stretched surface with a porous layer saturated with a Casson fluid is the aim of this work. The study explores the thermal conduction of nanofluids, taking into account the effects of thermal radiation, as well as the properties of thermophoresis parameter and Brownian motion.

Motivation

Some motivation points are described as:

- The rising demand for enhanced thermal efficiency in industrial and engineering applications, such as cooling systems, biomedical devices, and energy technologies, underscores the importance of studying the heat transfer properties of nanofluids.
- Despite the wide applicability of non-Newtonian fluid models, the Casson fluid model remains underexplored in scenarios involving unsteady stretched surfaces and Stefan blowing/suction, necessitating further investigation.
- Phenomena such as Brownian motion and thermophoresis significantly impact the thermal and concentration profiles of nanofluids but require a deeper understanding in the context of complex fluid models like Casson.
- Magnetic fields and unsteady flow conditions are crucial in regulating fluid dynamics in advanced applications, but their combined influence on Casson nanofluid systems remains an open question.

Research questions

The following research questions are described below:

- How do the unique thermal and flow properties of Casson nanofluid enhance heat transfer efficiency in engineering systems subjected to unsteady stretched surfaces?
- What is the impact of Casson fluid parameters on velocity, temperature, and concentration profiles under the influence of Stefan blowing/suction?
- How do Brownian motion and thermophoresis affect the thermal conductivity and nanoparticle concentration in Casson nanofluid flows?
- What is the combined effect of magnetic fields and unsteadiness parameters on the flow behavior and heat transfer characteristics of Casson nanofluid?

FORMULATION OF THE PROBLEM

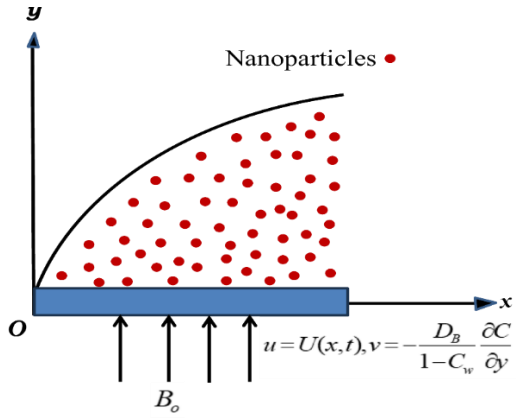

Fig. 1. Geometry of the problem.

Consider the unsteady hydromagnetic flow of electrically conducting Casson nanofluid across a stretching sheet. Magnetic field B_0 is applied perpendicularly to the surface. The schematic diagram presented in Fig. 1 depicts a complex network of interconnected elements, each playing a vital role in the overall functionality of the system. We may represent the dynamics of this system using a variety of techniques if we assume that a sheet starts stretching along the *x*-axis at time $t=0$ with velocity $U(x,t)=\frac{ax}{1-\alpha t}$ where the *y*-axis is orthogonal to the sheet. We consider the impacts of Lewis number and Stefan blowing/ suction. Chemical reactions, thermophoresis, and thermal radiations are closely intertwined phenomena that play an important part in many scientific and industrial applications. The Casson nanofluid [10, 26] rheological model is given by:

$$\tau_{ij}=\begin{cases}\left(\mu_b+\frac{P_y}{\sqrt{2\pi}}\right)2\varsigma_{ij}, & \pi>\pi_c\\ \left(\mu_b+\frac{P_y}{\sqrt{2\pi_c}}\right)2\varsigma_{ij}, & \pi<\pi_c\end{cases} \quad (1)$$

where ς_{ij}, τ_{ij}, P_y, and μ_b are deformation tensor, stress tensor, yield stress and plastic dynamic viscosity of the Casson fluid, respectively. The governing boundary layer equations under these presumptions can be written as [7, 9]:

$$\frac{\partial u}{\partial x}+\frac{\partial v}{\partial y}=0 \quad (2)$$

$$\frac{\partial u}{\partial t}+u\frac{\partial u}{\partial x}+v\frac{\partial u}{\partial y}=\upsilon\left(1+\frac{1}{\beta^*}\right)\frac{\partial^2 u}{\partial y^2}-\frac{\sigma B_o^{\,2}}{\rho}u-\frac{C_b}{\sqrt{k_0(t)}}u^2 \quad (3)$$

$$\frac{\partial T}{\partial t}+u\frac{\partial T}{\partial x}+v\frac{\partial T}{\partial y}=\frac{\kappa}{(\rho c_p)_f}\frac{\partial^2 T}{\partial y^2}+\frac{(\rho c_p)_p}{(\rho c_p)_f}\left[D_B\frac{\partial C}{\partial y}\frac{\partial T}{\partial y}+\frac{D_T}{T_\infty}\left(\frac{\partial T}{\partial y}\right)^2\right] \quad (4)$$
$$+\frac{\mu}{(\rho c_p)_f}\left(1+\frac{1}{\beta^*}\right)\left(\frac{\partial u}{\partial y}\right)^2-\frac{1}{(\rho c_p)_f}\frac{\partial q_r}{\partial y}$$

$$\frac{\partial C}{\partial t}+u\frac{\partial C}{\partial x}+v\frac{\partial C}{\partial y}=D_B\frac{\partial^2 C}{\partial y^2}+\frac{D_T}{T_\infty}\frac{\partial^2 T}{\partial y^2}-k_r(t)(C-C_\infty) \quad (5)$$

Boundary condition:

$$\left.\begin{aligned}&u=U(x,t), v=-\frac{D_B}{1-C_w}\frac{\partial C}{\partial y}, T=T_w, C=C_w \text{ at } y=0\\ &u\to 0, T\to T_\infty, C\to C_\infty \text{ at } y\to\infty\end{aligned}\right\} \quad (6)$$

Here the velocity components in the *x*- and *y*-axis directions are denoted by *u* and *v*, respectively, D_B is the coefficient of Brownian diffusion, $k_0(t)=k(1-\alpha t)$ is a time-dependent permeability parameter, $k_r(t)=k(1-\alpha t)^{-1}$ is a chemical reaction parameter, *k* is a constant, *t* denotes time, α is positive constant, $a>0$ be any constant, μ is dynamic viscosity, ν is kinematic viscosity, $\beta^*=\frac{\mu_b\sqrt{2\pi_c}}{P_y}$ is Casson fluid parameter, σ is electrical conductivity, D_F is coefficient of thermophoresis diffusion, κ is thermal conductivity, $(\rho c_p)_p$ is heat capacity of the nanoparticle material, C_b is a form of drag coefficient, π_c is the critical value of π, $\pi=\varsigma_{ij}^{\,2}$ is the result of multiplying ς_{ij} by itself, $(\rho c_p)_f$ is heat capacity of the fluid, *C* is concentration, ρ̇ is density of the fluid, $q_r=-\left(\frac{4\sigma^*}{3\chi}\right)\frac{\partial T^4}{\partial y}$ is radiative heat flux, σ^* is Stefan-Boltzmann constant.

$T^4 \cong 4T_\infty^3 T - 3T_\infty^4$ (Higher-order terms are neglected), T is temperature, T_w is surface temperature, C_w is surface nanoparticle concentration, χ is Rosseland mean absorption coefficient, T_∞ and C_∞ are the temperature and nanoparticle concentration distant from the exterior.

On simplifying Eq. (4), we get:

$$\frac{\partial T}{\partial t}+u\frac{\partial T}{\partial x}+v\frac{\partial T}{\partial y}=\frac{\kappa}{(\rho c_p)_f}\frac{\partial^2 T}{\partial y^2}+\frac{(\rho c_p)_p}{(\rho c_p)_f}\left[D_B\frac{\partial C}{\partial y}\frac{\partial T}{\partial y}+\frac{D_T}{T_\infty}\left(\frac{\partial T}{\partial y}\right)^2\right] \quad (7)$$
$$+\frac{\mu}{(\rho c_p)_f}\left(1+\frac{1}{\beta^*}\right)\left(\frac{\partial u}{\partial y}\right)^2+\frac{1}{(\rho c_p)_f}\frac{16\sigma^* T_\infty^3}{3\chi}\frac{\partial^2 T}{\partial y^2}$$

The skin friction coefficient (C_f), and the rates of mass and heat transfer (Sh_x, Nu_x) can be described as:

$$C_f=\frac{\tau_w}{\rho U^2},\ Nu_x=\frac{xq_w}{\kappa(T_w-T_\infty)},\ Sh_x=\frac{xq_m}{D_B(C_w-C_\infty)} \quad (8)$$

The surface mass and heat fluxes, shear stress near the wall are:

$$\left.\begin{aligned} q_m&=-D_B\left(\frac{\partial C}{\partial y}\right)\Big|_{y=0},\ q_w=-\kappa\left(\frac{\partial T}{\partial y}\right)\Big|_{y=0},\\ \tau_w&=\mu\left(1+\frac{1}{\beta^*}\right)\left(\frac{\partial u}{\partial y}\right)\Big|_{y=0}\end{aligned}\right\} \quad (9)$$

Now, we present the similarity variable η and the dimensionless functions g, θ, and ϕ as:

$$\psi=x\sqrt{\frac{a\upsilon}{(1-\alpha t)}}\mathrm{g}(\eta),\ \theta(\eta)=\frac{T-T_\infty}{T_\omega-T_\infty},\ \phi(\eta)=\frac{C-C_\infty}{C_\omega-C_\infty},\ \eta=y\sqrt{\frac{a}{\upsilon(1-\alpha t)}} \quad (10)$$

where ψ stands for stream function and is represented by the relationship that follows:

$$u=\frac{\partial\psi}{\partial y}\quad v=-\frac{\partial\psi}{\partial x} \quad (11)$$

Substituting Eqs. (10) and (11) into Eqs. (3), (7), and (5), we obtain the nonlinear ordinary differential equations:

$$\left(1+\frac{1}{\beta^*}\right)\mathrm{g}'''+\mathrm{g}''\mathrm{g}-A\left(\mathrm{g}'+\frac{\mathrm{g}''\eta}{2}\right)-M\,\mathrm{g}'-(1+Fs)(\mathrm{g}')^2=0 \quad (12)$$

$$\frac{1}{Pr}\left(1+\frac{4}{3}R_d\right)\theta''+\left(1+\frac{1}{\beta^*}\right)Ec(\mathrm{g}'')^2-\frac{A}{2}\eta\theta'+\mathrm{g}\theta'+Nb\,\theta'\phi'+Nt\,\theta'^2=0 \quad (13)$$

$$\phi''-LePr\left[\left(\frac{A}{2}\eta-\mathrm{g}\right)\phi'+\Gamma\phi\right]+\frac{Nt}{Nb}\theta''=0 \quad (14)$$

The renovated boundary constraints are:

$$\left.\begin{aligned} &\mathrm{g}'(\eta)=1,\ \mathrm{g}(\eta)=\frac{S_0}{Le}\phi'(\eta),\ \theta(\eta)=1,\ \phi(\eta)=1\ \ at\ \ \eta=0\\ &\mathrm{g}'(\eta)=0,\ \theta(\eta)=0,\phi(\eta)=0\ \ as\ \ \eta\to\infty\end{aligned}\right\} \quad (15)$$

where $Le=\frac{\alpha_0}{D_B}$ (Lewis number), $\alpha_0=\frac{\kappa}{(\rho c_p)_f}$ (thermal diffusivity), $Nb=\frac{(\rho c_p)_p D_B(C_w-C_\infty)}{(\rho c_p)_f\upsilon}$ (Brownian motion), $Nt=\frac{(\rho c_p)_p D_T(T_w-T_\infty)}{(\rho c_p)_f T_\infty\upsilon}$ (thermophoresis parameter), $\mathrm{Pr}=\frac{\mu c_p}{\kappa}$ (Prandtl number), $A=\frac{\alpha}{a}$ (unsteadiness parameter), $M=\frac{\sigma B_0^2(1-\alpha t)}{\rho a}$ (magnetic field parameter), $R_d=\frac{4\sigma^* T_\infty^3}{\chi\kappa}$ (radiation parameter), $Ec=(ax/1-\alpha t)^2/\left[c_p(T_w-T_\infty)\right]$ (Eckert number), $\Gamma=\frac{k}{a}$ (chemical reaction parameter), $Fs=\frac{C_b}{\sqrt{k_0(t)}}x$ (local inertia parameter), $S_0=\frac{C_w-C_\infty}{1-C_w}$ (Stefan blowing parameter) where $S_0 < 0$ and $S_0 > 0$ correspond to suction and blowing, respectively.

On simplifying Eq. (8), we get:

$$C_f\,\mathrm{Re}_x^{0.5}=\left(1+\frac{1}{\beta^*}\right)\mathrm{g}''(0),\ Nu_x\,\mathrm{Re}_x^{-0.5}=-\theta'(0),\ Sh_x\,\mathrm{Re}_x^{-0.5}=-\phi'(0) \quad (16)$$

where Reynolds number is denoted as $\mathrm{Re}_x=\frac{Ux}{\nu}$.

NUMERICAL SOLUTION

In our MATLAB computational approach, we utilized the bvp4c algorithm to solve dimensionless non-linear differential equations (12-14) alongside their corresponding boundary constraint (15). This involves employing the bvp4c solver within the MATLAB environment to derive numerical solutions for the ordinary differential equations. We first transformed the dimensionless non-linear ODEs into a first-order initial boundary value problem to streamline this process. The ensuing procedure delineates the necessary steps for obtaining the numerical solution:

$$\mathrm{g}=h_1,\ \mathrm{g}'=h_2,\ \mathrm{g}''=h_3,\ \theta=h_4,\ \theta'=h_5,\ \phi=h_6,\ \phi'=h_7 \quad (17)$$

$$h_3'=\frac{1}{\left(1+\frac{1}{\beta^*}\right)}\left[-h_3h_1+A\left(h_2+\frac{h_3\eta}{2}\right)+(1+Fs)(h_2)^2+M\,h_2\right] \quad (18)$$

$$h_5'=\frac{Pr}{\left(1+\frac{4}{3}R_d\right)}\left[-\left(1+\frac{1}{\beta^*}\right)Ec(h_3)^2+\frac{A}{2}\eta\,h_5-h_1h_5-Nb\,h_5h_7-Nt\,h_5^2\right] \quad (19)$$

$$h_7'=LePr\left[\left(\frac{A}{2}\eta-h_1\right)h_7+\Gamma h_6\right]-\frac{Nt}{Nb}h_5' \quad (20)$$

Boundary conditions are:

$$\left.\begin{aligned} &h_2 = 1,\ h_1 = \left(S_0 / Le\right) h_7,\ h_4 = 1,\ h_6 = 1 \quad at\ \ \eta = 0 \\ &h_2 = 0,\ h_4 = 0,\ h_6 = 0 \qquad\qquad\qquad at\ \ \eta = \infty \end{aligned}\right\} \quad (21)$$

RESULTS AND DISCUSSION

Chemical reaction and non-Darcian porous medium were taken into consideration while analyzing the Stefan blowing effect in a Casson nanofluid *via* stretched sheet. Numerical techniques and similarity transformations were used to define and solve the governing equations. The findings were displayed in tables and graphs that show how important factors affect the profiles of temperature, velocity, and concentration. The influence of Casson fluid parameter β^* on the velocity field is shown in Figure 2. The observed augmentation in the velocity profile, concomitant with an increase in the Casson nanofluid parameter, unveils a complex interplay of rheological characteristics and momentum transport within the fluid system. Figure 3 delineates that a rise in Forchheimer number creates a resistance in fluid flow which results in abatement on velocity. The velocity significantly decreases when the magnetic field parameter M increases, as Figure 4 illustrates. This is because of the Lorentz force which opposes the fluid motion by acting as a resistive drag. The fluid's velocity decreases more dramatically as the magnetic field intensity rises because the opposing force also gets greater. Figure 5 depicts that the speed of the liquid rises for dissimilar rising data for the Stefan suction/blowing parameter S_0 for both steady and unsteady flows. The injection of miniature rudiments throughout the edge regenerates the dispersion of species. On the other hand, the transfer of miniature rudiments slows down dispersion, so increasing values of injection cause an enlargement of the speed of the liquid.

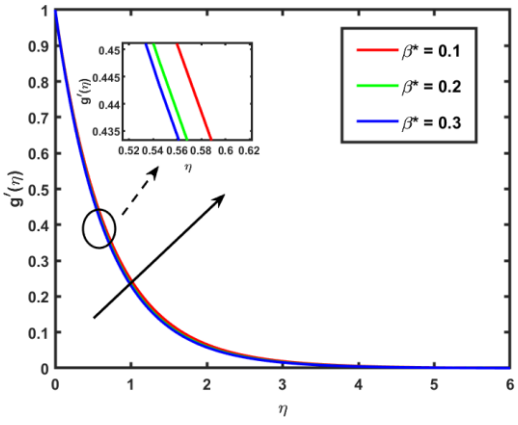

Fig. 2. Velocity fields with rising β^*.

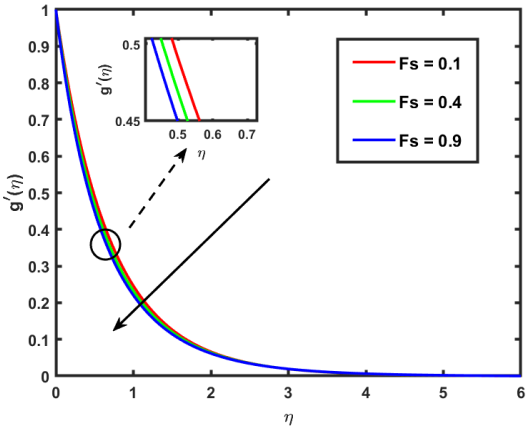

Fig. 3. Velocity fields with rising Fs .

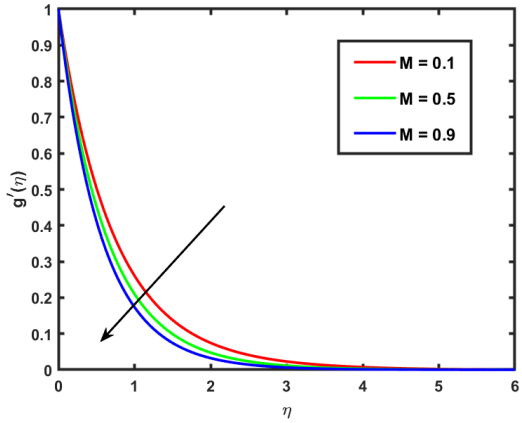

Fig. 4. Velocity fields with rising M .

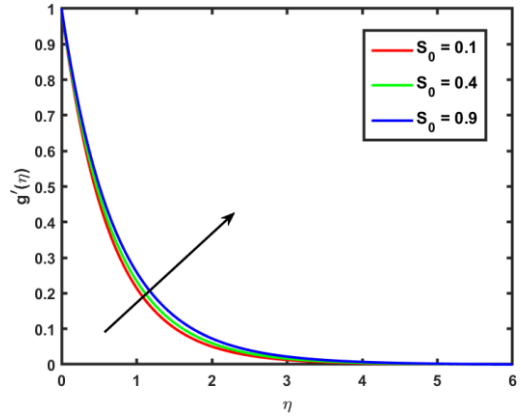

Fig. 5. Velocity fields with rising S_0 .

Figure 6 illustrates that the temperature distribution rises when the Casson fluid parameter β^* increases. Thickening of the thermal border coating takes place owing to amplification in the elasticity stress parameter. As seen in Figure 7, the temperature progressively rises as the Brownian motion parameter Nb increases. The random movement of nanoparticles is enhanced by Brownian motion which accelerates thermal energy transfer and raises the temperature. A rise in the

radiation parameter R_d, as Figure 8 illustrates, causes the temperature field to increase. This is because stronger radiation makes the fluid more capable of absorbing and releasing thermal energy, which boosts the temperature distribution and total heat transfer.

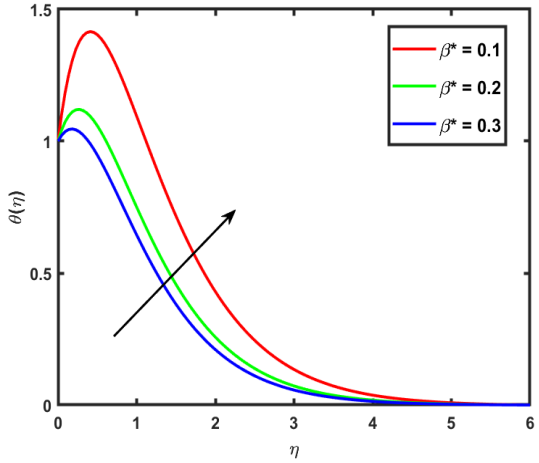

Fig. 6. Temperature fields with rising β*.

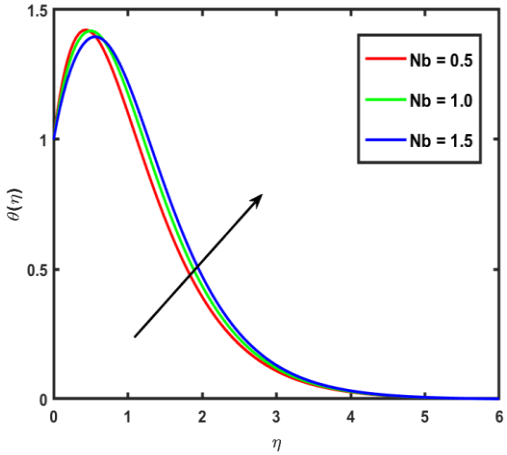

Fig. 7. Temperature fields with rising Nb.

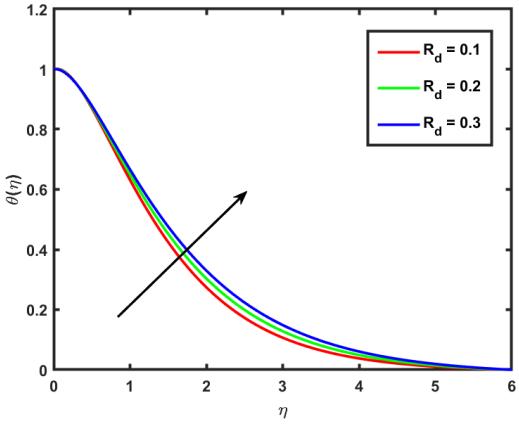

Fig. 8. Temperature fields with rising R_d.

The influence of unsteady parameter A on the concentration field is shown in Figure 9. The unsteadiness increases mass diffusion, which raises nanoparticle dispersion and causes concentration to rise dramatically. These impacts demonstrate how uneven flow alters the dynamics of mass movement. Figure 10 shows that a large drop in the concentration field occurs when the chemical reaction parameter Γ increases. This is because chemical species are consumed more quickly at a higher reaction rate, which lowers the concentration of those species overall in the border layer. Figure 11 demonstrates that a large drop in the concentration field occurs when the Lewis number Le is increased. One can observe that ϕ is a decreasing function of Le. This may be due to the fact that increasing of Lewis number increases mass transfer rate and hence nanoparticle concentration decreases. Figure 12 illustrates how a minor increase in the Stefan blowing parameter S_0 raises the concentration. A slow increase in concentration results from the improved mass transport close to the surface.

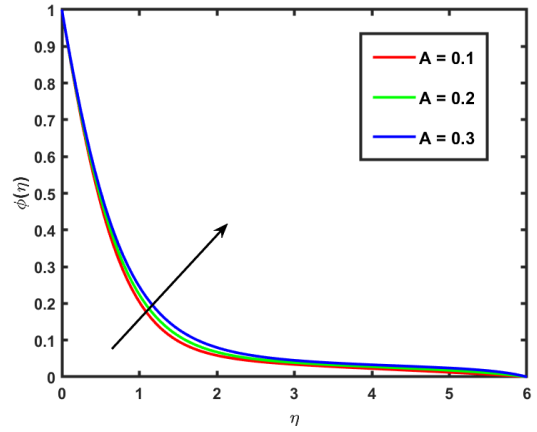

Fig. 9. Concentration fields with rising A.

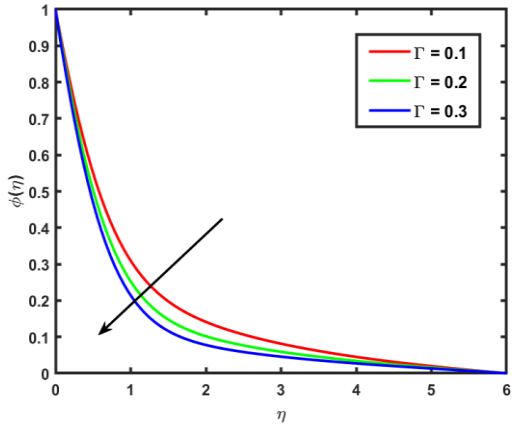

Fig. 10. Concentration fields with rising Γ.

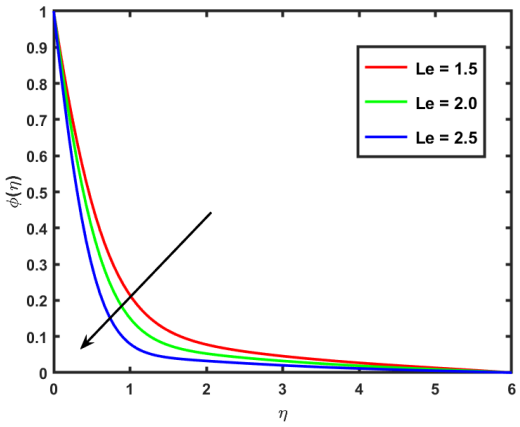

Fig. 11. Concentration fields with rising Le.

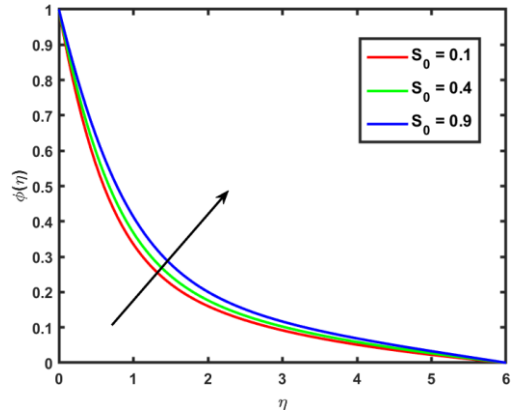

Fig. 12. Concentration fields with rising S_0.

Table 1. Values of -g"(0) for different values of Casson fluid parameter β^*.

β^*	Prasad *et al.* [26]	Konai *et al.* [9] for $S_0 = A = 0$	Present result for $S_0 = A = 0$
1.0	0.707107	0.707220	0.707109
2.0	0.816497	0.816540	0.816544
5.0	0.912871	0.912889	0.912883
$\beta^*=\infty$ (Newtonian fluid)	1.000000	1.000010	1000030

Table 2. Values of $C_f \,\mathrm{Re}_x^{0.5}$, $Nu_x \,\mathrm{Re}_x^{-0.5}$ and $Sh_x \,\mathrm{Re}_x^{-0.5}$ with $M = 0.2$, $\mathrm{Pr} = 21$, $Nb = 0.1$, $Le = 1.5$, $Nt = 0.1$, $R_d = 0.1$, $\Gamma = 0.5$, $Fs = 0.4$, and $Ec = 0.1$.

Parameter	Value	$C_f \,\mathrm{Re}_x^{0.5}$	$Nu_x \,\mathrm{Re}_x^{-0.5}$	$Sh_x \,\mathrm{Re}_x^{-0.5}$
S_0	0.1	-1.064138	-0.351360	-1.129400
	0.3	-1.024300	-0.289400	-0.982365
	0.5	-0.988634	-0.186962	-0.923577
A	0.1	-0. 548820	-0. 406490	-0. 600590
	0.2	-0. 555342	-0. 380746	-0. 537396
	0.3	-0. 573670	-0. 342618	-0. 470684
β^*	1.0	-0. 805948	-0.450407	-0. 592327
	2.0	-0. 855042	-0.396210	-0.575154
	3.0	-0. 901867	-0. 376084	-0. 559645

The comparison shown in Table 1 validates the computational technique by demonstrating great agreement between the current numerical results and earlier research. Moreover, the findings in Table 2 demonstrate how important factors affect the gradients in temperature, concentration, and velocity. The rising temperature and concentration gradients show that increasing the Stefan blowing parameter S_0 promotes heat and mass transmission while modestly increasing velocity. The rising mass and heat transfer rates show that increasing the unsteadiness parameter A promotes heat and mass transmission while modestly decreasing velocity. Likewise, the Casson fluid parameter β^* indicates a general improvement in thermal and solutal transport by strengthening the velocity gradient and slightly raising temperature and concentration levels.

CONCLUSIONS

This work explores the behavior of a Casson nanofluid flowing over an expanding surface, looking at mass transference and heat transference rate *via* physical experimentation and numerical simulations. The heat transfer rate also displays notable variability in response to alterations in the Stefan blowing parameter. Numerical results are derived using the bvp4c by MATLAB software to solve the ordinary differential system. Stefan blowing parameter indicates a qualitative similarity between velocity and concentration profiles. For greater *Fs*, g'(η) indicates a diminishing tendency, but for Casson fluid parameter β^*, the reverse trend is observed. The concentration field of the boundary layer could change significantly as a result of a chemical reaction. The thickness of the solutal boundary layer significantly decreases as the chemical reaction increases. The intricate interplay between chemical reactions and boundary layer dynamics constitutes a pivotal area of research with profound implications across diverse scientific and engineering domains. Higher Lewis numbers *Le* indicate a dominance of thermal diffusivity over mass diffusivity, resulting in faster heat transfer but slower concentration adjustments. This finding underscores the importance of controlling the Lewis number *Le* to balance thermal and mass transfer in practical applications. Skin friction decreases for fluid parameter β^* and boosts up for the Stefan blowing parameter S_0.

Future directions

The work can be modified by adding the impact of motile microorganisms, different nanoparticles, activation energy, thermal radiation and shaped change.

REFERENCES

1. N. Casson, in: Rheology of Disperse Systems, C.C. Mills (ed.), Pergamon, New York, 1959, p. 84.
2. R. K. Dash, K. N. Mehta, G. Jayaraman, *Int. J. Eng. Sci.*, **34**(10), 1145 (1996).
3. S. Srinivas, C. K. Kumar, A. S. Reddy, *Nonlinear Anal. Mod. Control*, **23**(2), 213 (2018).
4. M. Usman, F. A. Soomro, R. U. Haq, W. Wang, O. Defterli, *Int. J. Heat Mass Transfer*, **122**, 1255 (2018).
5. T. Hayat, S. A. Khan, S. Momani, *Int. J. Hydro. Ener.*, **47**(12), 8048 (2022).
6. A. Shateri, A. M. Ganji, P. Jalili, B. Jalili, D. D. Ganji, *Res. Eng.*, **25**, 103760 (2025).
7. C. K. Kumar, S. Srinivas, *Special Top. Rev. Porous Media*, **10** (4), 385 (2019).
8. M. A. Z. Raja, K. S. Nisar, M. Shoaib, M. Abukhaled, A. Riaz, *Heliyon*, **9**(10), e20911 (2023).
9. S. Konai, H. Maiti, S. Mukhopadhyay, *Force Mech.*, **12**, 100227 (2023).
10. M. S. Sankari, M. E. Rao, W. Khan, M. H. Alshehri, S. M. Eldin, S. Iqbal, *Case Stud. Therm. Eng.*, **50**, 103492 (2023).
11. S. G. Elgendi, W. Abbas, A. A. M. Said, A. M. Megahed, E. Fares, *J. Nonlinear Math. Phys.*, **31**, 19 (2024).
12. A. Kumar, D. Bhargavi, K. Vajravelu, *Phys. Fluids*, **37**(2), 023132 (2025).
13. S. S. Ghadikolaei, M. Yassari, H. Sadeghi, Kh. Hosseinzadeh, D. D. Ganji, *Powder Tech.*, **322**, 428 (2017).
14. C. K. Kumar, S. Srinivas, *Heat Transf.*, **50**(6), 5225 (2021).
15. S. Srinivas, K. K. Challa, S. Badeti, P. B. Kumar, *Eng. Trans.*, **71**(4), 519 (2023).
16. M. S. Sankari, M. E. Rao, F. A. Awwad, E. A. A. Ismail, O. D. Makinde, W. Khan, *Front. Chem.*, **12**, 1451053 (2025).
17. A. Pantokratoras, *Int. J. Heat. Mass Transf.*, **51**(1-2), 104 (2008).
18. M. R. Mishra, S. M. Hussain, O. D. Makinde, G. S. Seth, *Bul. Chem. Comm.*, **52**(2), 259 (2020).
19. S. M. A. Haider, B. Ali, Q. Wang, C. Zhao, *Coatings*, **11**, 1048 (2021).
20. A. M. Alqahtani, M. Bilal, M. Usman, T. R. Alsenani, A. Ali, S. R. Mahmoud, *Z. Angew. Math. Mech.*, **103**, e202200213 (2023).
21. D. Thenmozhi, M. Eswara Rao, *Prop. Power Res.*, **13**(2), 257 (2024).
22. Y. Ouyang, Md F. Md Basir, K. Naganthran, I. Pop, *Alex. Eng. J.*, **116**, 427 (2025).
23. S. Idris, A. Jamaludin, R. Nazar, I. Pop, *Chin. J. Phys.*, **93**, 611 (2025).
24. S. M. Hussain, J. Jain, G. S. Seth, *Bul. Chem. Comm.*, **48**(4), 659 (2016).
25. M. Eswara Rao, S. Sreenadh, *Global J. Pure Appl. Math.*, **13**, 7529 (2017).
26. K. V. Prasad, K. Vajravelu, H. Vaidya, N. Z. Basha, V. Umesh, *Ain Shams Eng. J.*, **9**(4), 1763 (2017).
27. A. S. Reddy, K. K. Challa, S. Srinivas, T. R. Ramamohan, K. Vajravelu, *Ind. J. Chem. Tech.*, **31**, 186 (2024).
28. D. Thenmozhi, M. Eswara Rao, RLV. R. Devi, Ch. Nagalakshmi, PD. Selvi, *Int. J. Thermofluids*, **24**, 100896 (2024).
29. S. Kosar, M. Sagheer, S. Hussain, *Int. J. Modern Phy. B*, **39**(01), 2550002 (2025).
30. N. A. M. Noor, S. Shafie, M. A. Admon, *J. Adv. Res. Fluid Mech. Therm. Sci.*, **68**(2), 94 (2020).
31. P. T. Manjunatha, A. J. Chamkha, R. J. P. Gowda, R. N. Kumar, B. C. Prasannakumara, S. M. Naik, *J. Nanofluids*, **10**, 285 (2021).
32. A. Abbasi, S. U. Khan, K. Al-Khaled, M. I. Khan, W. Farooq, A. M. Galal, K. Javid, M. Y. Malik, *Chem. Phys. Lett.*, **786**, 139172 (2022).
33. Z. Khan, H. U. Rasheed, I. Khan, H. Abu-Zinadah, M. A. Aldahlan, *Materials*, **15**(3), 747 (2022).
34. S. Srinivas, C. K. Kumar, S. Badeti, A. S. Reddy, *Springer Nature, Singapore*, **155** (2023).
35. S. Saleem, T. Abbas, H. Abutuqayqah, E. U. Haq, S. U. Khan, *Alex. Eng. J.*, **79**, 629 (2023).
36. A. shateri, B. Jalili, S. Saffar, P. Jalili, D. D. Ganji, *Energy*, **289**, 129707 (2024).
37. R. Razzaq, Z. Khan, M. N. Abrar, B. Almohsen, U. Farooq, *Chaos, Soli. Frac.*, **190**, 115756 (2025).
38. Md. M. Hasan, M. J. Uddin, S. A. Faroughi, *Int. J. Thermofluids*, **26**, 101114 (2025).
39. E. R. M, K. K. Challa, T. D, M. Jawad, *Z Angew. Math. Mech.*, **105**, e70226 (2025).